Proc. of the XI Int. Conf. — Ion Implantation and other Applications of Ions and Electrons, Kazimierz Dolny 2016

Modification of Optical and Electrical Properties of PET Foils by He^+, Ne^+ and Ar^+ Implantation

A. Droździel[a], M. Turek[a,*], K. Pyszniak[a], S. Prucnal[a], R. Luchowski[a], W. Grudziński[a], A. Klimek-Turek[b] and J. Partyka[c]

[a]Institute of Physics, Maria Curie-Skłodowska University, Pl. M. Curie-Skłodowskiej 5, 20-031 Lublin, Poland
[b]Department of Physical Chemistry, Medical University of Lublin, W. Chodźki 4A, 20-093 Lublin, Poland
[c]Technical University of Lublin, Nadbystrzycka 38A, 20-618 Lublin, Poland

Thin (3 μm) polyethylene terephthalate (PET) foils were irradiated with 135 keV He^+, Ne^+ and Ar^+ ions with the fluences up to 5×10^{15} cm^{-2}. Changes of chemical structure of the polymer were studied with the Fourier transform infrared and Raman spectroscopy — breaking of numerous chemical bonds, polymer chain cross-linking as well as formation of sp^2 hybridised carbon clusters and cluster networks were demonstrated. The increase of the implanted sample absorbance with the implantation fluence in the UV-VIS spectra as well as the decrease of optical band-gap energy (2.75 and 2.0 eV for He and Ne, respectively, at 5×10^{15} cm^{-2}) are observed. Decrease of bulk resistance of heavily treated samples by ≈ 5 orders of magnitude is determined. Measurements of the sheet resistance confirm that the sample becomes conducting also on the reverse (unimplanted) side of the foil. Both of these effects depend on the impinging ion mass — they are the strongest for Ar. The increase of both ac conductance and dielectric constant is observed in the frequency range up to 2 MHz and these changes rise with the impinging ion mass.

DOI: 10.12693/APhysPolA.132.264
PACS/topics: 78.40.Me, 78.30.Jw, 61.82.Pv

1. Introduction

For many years polymers have attracted attention of scientists and engineers due to their unique properties, such as low cost, low density, plasticity etc. [1]. On the other hand, there are some limitations of their application related to their wear and chemical resistance as well as unpredictable electrical properties [2], mostly very high electrical resistance restricting their use in micro- and optoelectronics. Ion implantation is very effective tool enabling improvement of surface properties such as hardness and wear resistance [3, 4]. This method offers a very precise control of the distribution of the implanted dopant by altering the implantation parameters like energy and fluence [5]. Hence, ion implantation could be used for modification of surface properties of polymers without altering their bulk properties.

Bombardment by energetic ions induces a variety of processes in the subsurface layer resulting in modification of its physical and chemical properties. These include: bond breaking, cross linking, polymer chain scissions, gas release, carbonisation [6].

Changes of physical and chemical properties due to ion implantation in a variety of polymers were under investigation during last years. These include e.g. polyethylene (PE) [7–9], polycarbonate (PC) [10, 11], polymethylmethacrylate (PMMA) [12, 13] as well as polyethylene terephthalate (PET).

*corresponding author; e-mail: mturek@kft.umcs.lublin.pl

Polyethylene terephthalate $(C_{10}H_8O_4)_n$ is a highly transparent ($\approx 90\%$ in the visible region) thermoplastic polymer resin. It is a very popular polymer used widely for packaging purposes as well as fiber production [14, 15] but also for light fibre photographic filters and lens production etc. [16]. Numerous studies of PET samples irradiated by noble gases [17–22], metals [23–25] and non-metals [2,26] were reported. In most cases a very prominent decrease of PET resistance with the implantation fluence was shown. This is due to carbonisation of the polymer subsurface layer and appearance of carbon clusters forming a conducting network [22] or metal "islands" [23]. The intense irradiation (fluences $\approx 10^{16}$ cm^{-2} or even more) change the PET absorption spectra — shift of the absorption edge, as well as reduction of the optical band-gap energy are observed. The changes of the surface topography and wettability were also studied [27].

As the above described changes are the results of damage caused by ion bombardment, one may suspect that changes in bulk properties of the foil are more prominent in the case of very thin samples, as in the case described in this paper. When the implantation range is comparable to the foil thickness it is also feasible to determine a relative dielectric constant e.g. by capacitance measurements using capacitors filled with modified and virgin foils. The paper presents the studies of modification of very thin PET foil due to implantation of three different noble gas ions (He, Ne and Ar) — one of the aims was to compare differences caused by using projectiles of different mass. Structural modifications of the polymer are investigated using the Fourier transform infrared (FTIR) and Raman spectroscopy. Changes of foil transparency

are studied by the UV-VIS spectroscopy — change of the optical bandgap energy is shown. The results of measurement of both bulk and surface resistivity are presented. The paper also deals with the investigations of dielectric constant and ac conductivity modification due to the noble gas ions irradiation.

2. Experimental

Thin (thickness of 3 μm) PET (Hostaphan®, bi-axially oriented, ≈ 1.4 g/cm^3) foils were implanted with 135 keV beams of He^+, Ne^+ and Ar^+ ions using the UNIMAS implanter equipped with an arc discharge ion source [28, 29]. The PET foil was placed inside the cylindrical ring-shaped frames (internal diameter of ≈ 17 mm) in order to prevent it from folding and make all necessary manipulations easier. Implantations were performed with fluences of 10^{12}, 10^{13}, 5×10^{13}, 5×10^{14}, 5×10^{15} cm^{-3} at room temperature. The ion current density of 0.3 μA/cm^2 was maintained in all cases.

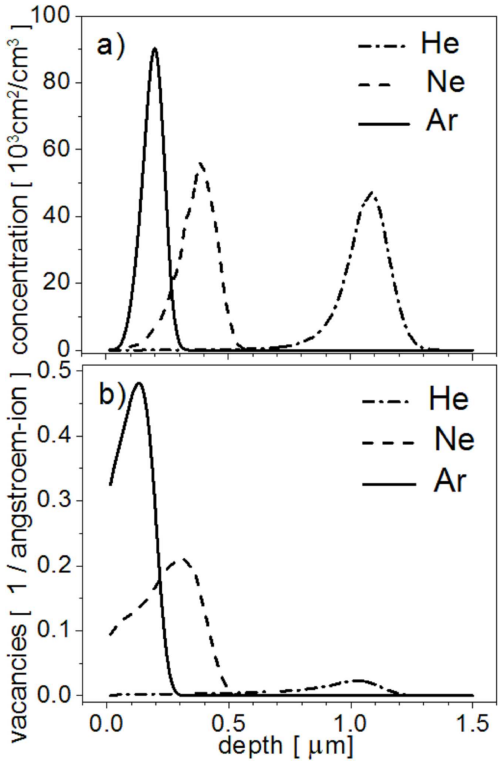

Fig. 1. Depth profiles of ions (He, Ne, and Ar) implanted into PET (E = 135 keV) (a) and distribution of produced vacancies calculated using the SRIM software (b).

The depth profiles as well as distributions of produced vacancies were calculated using the SRIM software [30]. The results are shown in Fig. 1. The average projected ranges of He, Ne, and Ar ions were 1049, 359, and 182 nm, whereas the corresponding stragglings were 110, 80, and 43 nm, respectively. The FTIR spectra were determined using the Nicolet iS50R spectrometer (ThermoScientific, USA). The absorbance spectra were measured in the UV-VIS-NIR range (200–1000 nm) using the Cary 50 (Agilent) spectrophotometer. The Raman spectra were collected by the inVia system (Renishaw, UK). Sheet resistivity of the samples was measured using the coaxial electrodes and the Agilent B2911A precision source/measure unit. Bulk resistivity of the PET samples and their other electrical parameters were determined employing the Hioki IM3570 impedance analyser and a set of polished circular electrodes.

3. Results

Chemical structure of implanted PET undergoes numerous changes as can be seen in the FTIR spectra in Fig. 2. The peaks at 722, 1016, 1340, and 1409 cm^{-1} which are fingerprints of C–H bonds decrease with the implantation fluence which can indicate occurrence of some additional groups as in the case of implanted polypropylene films [31]. Destruction of C–C–O bonds is also observed (peaks at 1103 cm^{-1} and 1252 cm^{-1}). The most prominent peak ($\approx$ 1714 cm^{-1}) in all spectra, i.e. that from the C=O bond in the carbonyl group also decreases with the fluence. Destruction of chemical bonds is also confirmed by the Raman spectra (Fig. 3). The most prominent peaks include 632 cm^{-1} C–C–C in-plane ring bending, 857 cm^{-1} C–C breathing, 1286 cm^{-1} ring plus O–C stretching, 1613 cm^{-1} C=C ring stretching and 1727 cm^{-1} C=O stretching [32]. For smaller fluences the changes in the spectra are small, minor reduction of characteristic peaks is observed. As the fluence increases above 10^{14} cm^{-2}, wide bands near 1000 cm^{-1} and 1600 cm^{-1} appear. Finally, peaks characteristic of the polymer disappear in the case of heavy implanted samples and the spectra are dominated by D and G bands as the Raman excitation cross-sections of sp^2 carbon atoms are larger than those of sp^3. The above mentioned very broad peaks appearing as a result of heavy ion bombardment could be assigned to the D and G bands of amorphous carbon resulting from breathing vibration of rings (D) and stretching vibration modes of both rings and chains (G) formed by sp^2 carbon atoms. It is known that sp^2 C atoms bond to each other preferentially, forming clusters (islands) in the sp^3 hybridised matrix [22]. These clusters are made mostly of chains and rings interconnected and crosslinked with each other. Due to the fact that rings contribute to both modes while chains to the G mode only, their relative strength can be an estimate of the content of two basic constituents in clusters [22]. As can be deduced from the spectra in Fig. 3b, He bombardment leads to more intense sp^2 rings formation while more carbon chains appear as a result of irradiation with heavier ions.

The increase of sample carbonisation can be seen as its darkening. The relationship between the sample colour and sp^2 carbon bands parameters was considered in [22]. The UV-VIS spectra in the range 300–700 nm are pre-

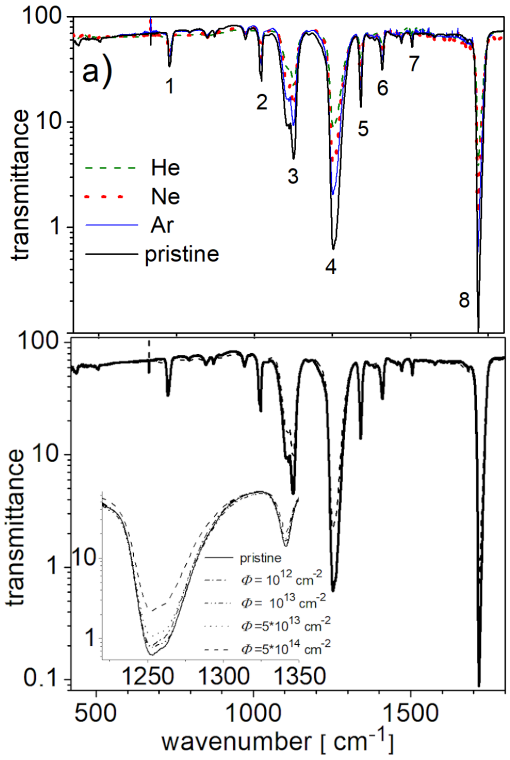

Fig. 2. FTIR spectra of the samples implanted with different ions and maximal fluence (a) and changes of the FTIR spectra with influence of Ne irradiations (b).

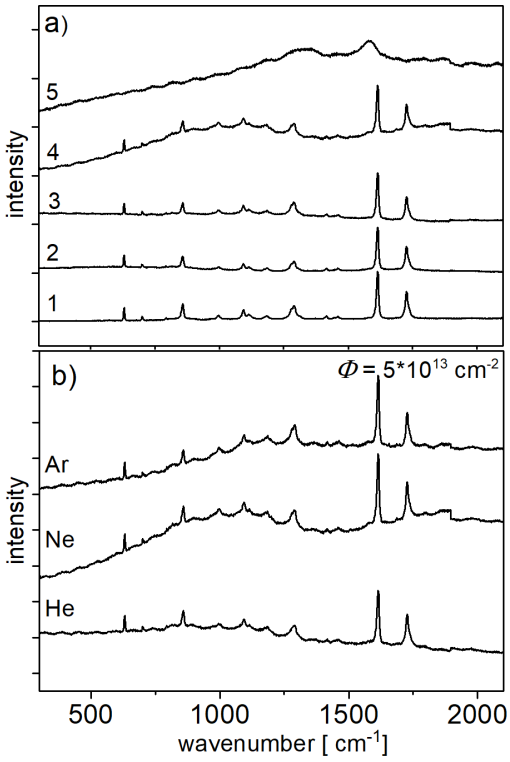

Fig. 3. Raman spectra for the samples implanted with different fluences of Ne ions (a) and the spectra for the samples implanted with different ions with $\Phi = 5 \times 10^{14}$ cm^{-2} (b).

sented in Fig. 4. The untreated foil is almost transparent in the visible region. For the implantation fluences larger than 10^{13} cm^{-2} a prominent increase of the absorbance is observed. Also shift of the absorption edge toward larger wavelengths is observed for larger implantation doses (above 10^{15} cm^{-2}) as in the case of implanted PMMA [13]. This shift is known to be related to the formation of carbon cluster network and, consequently, decrease of the optical bandgap of the irradiated sample [13, 18, 20, 21]. The optical bandgap E_0 could be estimated using the Tauc relation

$$\alpha h\nu \sim (h\nu - E_0)^2 , \quad (1)$$

where is the absorption coefficient. Then the optical bandgap can be estimated by plotting $(\alpha h\nu)^{1/2}$ vs. $h\nu$ and taking the interception of the linear part of the plot and the energy axis. The values of the bandgap energy for some implanted samples are gathered in Table I. The bandgap energy decreases with the implantation fluence for all ion species, though the impact of Ar implantation is surprisingly small. The bandgap energy in the case of $\Phi = 5 \times 10^{15}$ cm^{-2} is reduced to 2.0 eV (Ne) and 2.75 eV (He) compared to ≈ 3.95 eV of the pristine sample. As it was mentioned before this reduction is due to the structural deformation of polymer chains, formation of carbonaceous clusters and, consequently, appearance of lower-energy lying states due to the ion irradiation [13, 26].

As the result of ion implantation the polymer becomes

TABLE I

Optical bandgap values estimated from the Tauc formula (1) and mean number of carbon atoms in a cluster.

Φ [cm^{-2}]	E_0 [eV]			M		
	He	Ne	Ar	He	Ne	Ar
5×10^{13}	3.9	3.9	3.9	77	77	77
5×10^{14}	3.8	3.8	3.85	81	81	79
5×10^{15}	2.75	2.0	3.72	156	294	85

carbonised. The mean number of carbon atoms in a cluster could be estimated by the following equation [33]:

$$N = \left(\frac{34.3}{E_0\ [eV]} \right)^2 . \quad (2)$$

It can be seen that the number of C atoms in the cluster rises with the implantation fluence, and the observed effect is the strongest in the case of Ne bombardment. For smaller implantation well-conducting C clusters are rather isolated. However, as Φ increases, aggregation of clusters takes place. One may expect that forming a buried layer containing a vast percolation cluster of C atoms changes conductivity of the sample [18, 20].

This is also true in the case of the samples presented in this paper. Figure 5 shows the bulk conductivity of PET samples as a function of implantation fluence for three ion species. It should be mentioned that the no-

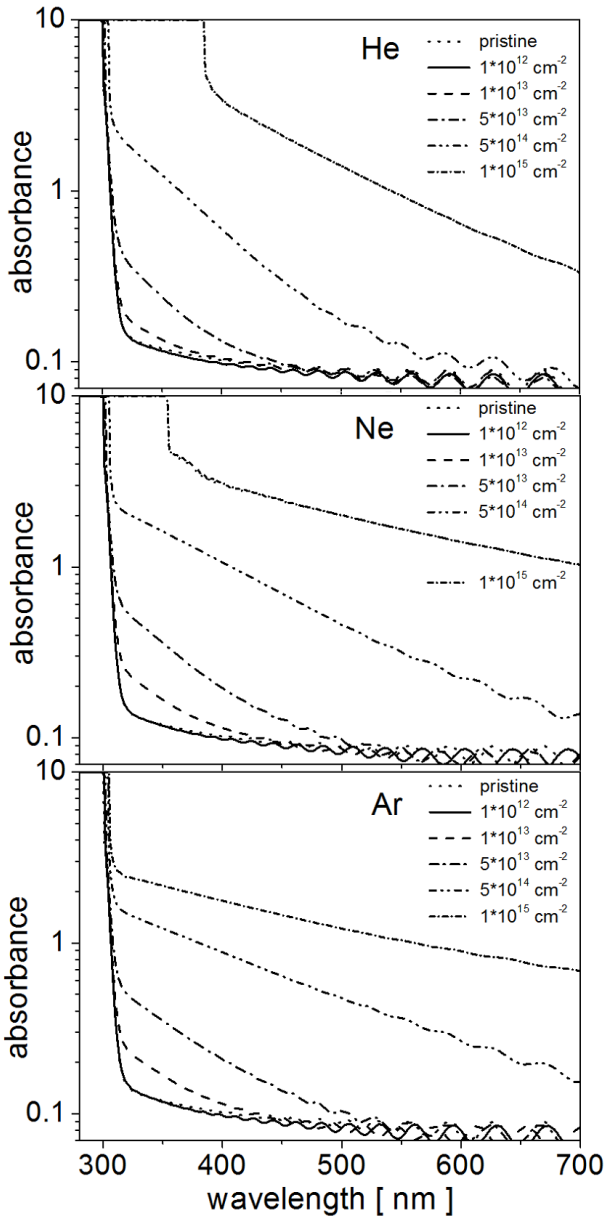

Fig. 4. UV-VIS absorbance spectra for the samples implanted with different fluences.

TABLE II

Sheet resistance for the sample implanted with $\Phi = 5 \times 10^{15}$ cm^{-2} measured on both sides of foils.

Side	Sheet resistance [Ω/□]		
	He	Ne	Ar
implanted	1.42×10^{10}	2.70×10^{9}	1.25×10^{9}
reverse	2.24×10^{13}	9.72×10^{12}	7.02×10^{12}

tion. The sheet resistance of the samples implanted with the maximal fluences was also measured. The results are given in Table II. Sheet resistance decreases with the ion mass. This can be also related to the above mentioned fact that the conducting graphite-like network is buried more deeply under the surface in the case of lighter ion irradiation. It should be stressed that sheet resistance of the reverse side of the foil is reduced in the case of high fluence implantation. This is, however, by ≈ two orders of magnitude larger than that of the implanted side. One of the possible explanations is that this is due to the raised temperature of the irradiated sample leading to chemical transformation in the whole bulk of very thin foil.

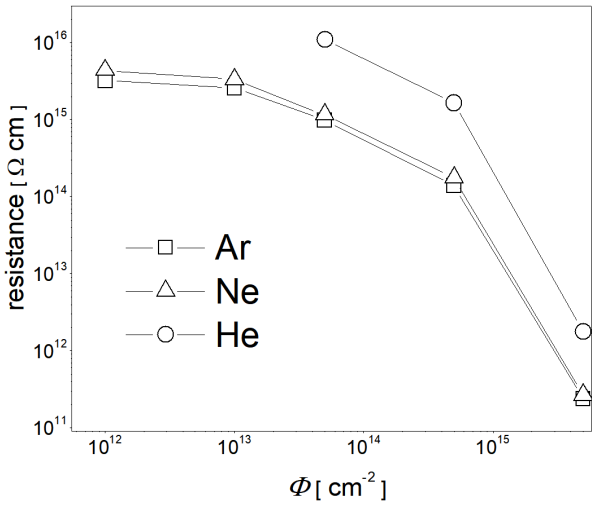

Fig. 5. Changes of PET foil bulk resistance with the implantation fluence for He, Ne and Ar ions.

tion of bulk resistivity modification is more justified in the case of a very thin sample (as in the considered case) when the projected range is comparable to the sample thickness. One can see that the resistance of the sample decreases fast with the implantation fluence, by ≈ 5 orders of magnitude in the considered Φ range. This effect is especially dramatical when Φ is larger than 10^{15} cm^{-2} . The observed behaviour is very similar to the results observed for implantations with noble gas ions [18–21], metals [23, 34] and non-metals [2, 26]. Higher measured resistance of the He implanted sample can be a result of the fact that the conducting layer is buried more deeply than that produced in the case of heavier ion implanta-

Measurements of ac conductance of implanted samples were performed for the frequencies up to 2 MHz. The results are shown in Fig. 6. Generally, the conductance increases with Φ in the considered frequency range and the $G-f$ curves for lower Φ follow the Jonscher power law [35] $G = a + bf^s$ for high frequencies and their trend resembles the response of conducting polymers or glasses [36, 37]. The deviation from the assumed plateau for lower frequencies is most probable due to the electrode polarisation effect. However, the shape of conductance curves for heavily treated samples differs much from that described by the power law.

Modification of the real part of electric constant was

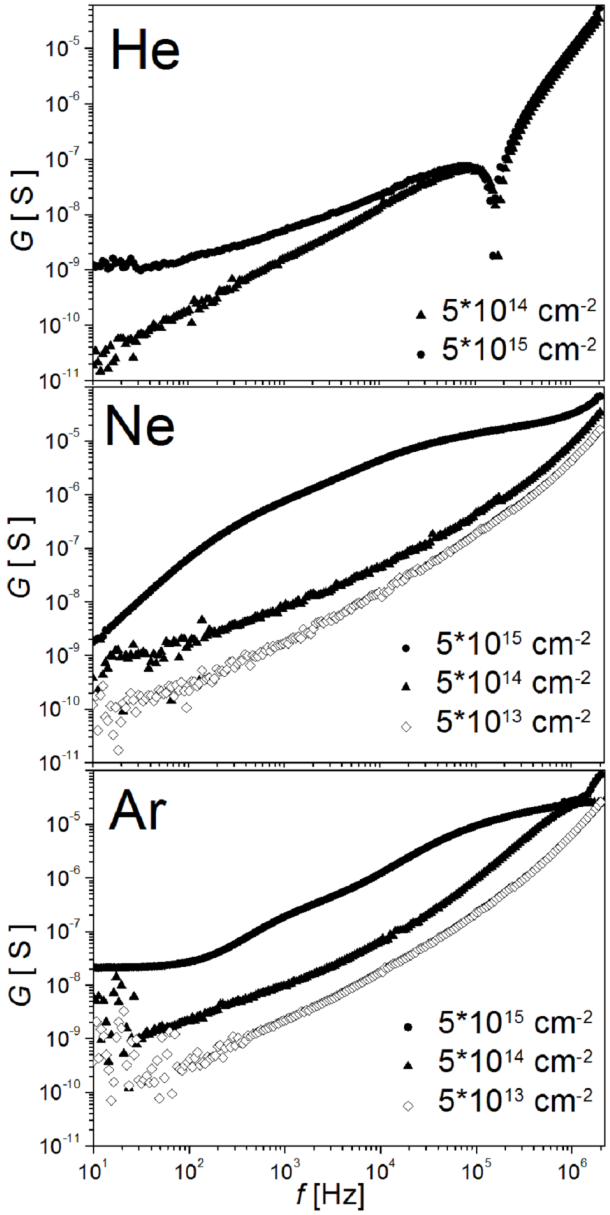

Fig. 6. Changes of ac conductance of the samples irradiated with different fluences of He, Ne and Ar ions.

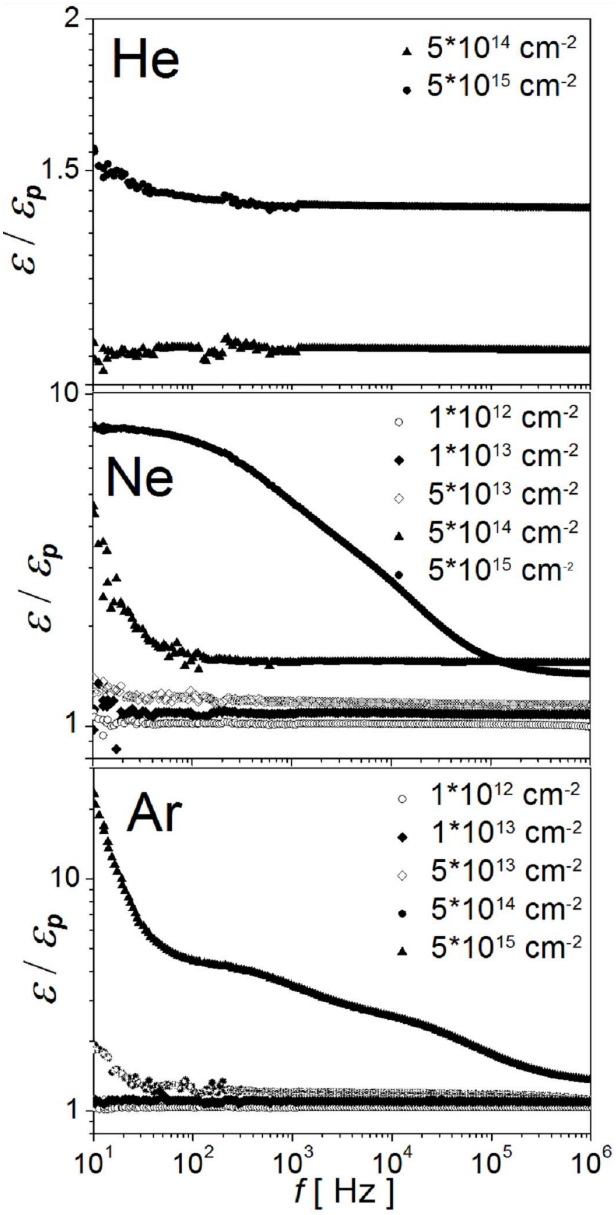

Fig. 7. Changes of the relative dielectric constant of the PET samples implanted with different fluences of He, Ne and Ar ions.

measured by comparing the capacities of the condenser filled with the implanted and pristine samples. The results are shown in Fig. 7. One can see that the heavier projectile ions, the larger is the impact on the relative dielectric constant reaching the values 8 and 12 in the case of Ne and Ar, respectively. Strong frequency dispersion can be seen for the samples Ar and Ne implanted with the doses above 10^{14} cm^{-2}. For higher frequencies the curves are flat, and the dielectric constant at plateau increases with the implantation fluence (Fig. 7).

4. Conclusions

Modification of some structural, optical and electrical properties of PET foils due to the noble gas (He, Ne, and Ar) ion implantation (135 keV) with the fluences up to 5×10^{15} was under investigation. The Raman and FTIR spectroscopy spectra showed that the degree of destruction of different bonds in the polymer molecules rises with the implantation fluence. Formation of carbon clusters composed of sp^2 hybridised atoms is indicated by the presence of wide D and G bands characteristic of the amorphous carbon structures. With the increasing implantation fluence carbon clusters tend to form a vast network. This leads to the increasing electrical conductivity of the irradiated samples — even by 5 orders of magnitude for largely modified samples. This effect is stronger for heavier ions. It was also shown that the sheet resistance of the implanted foils is reduced. Moreover, af-

ter irradiation the samples become conducting (although with the sheet resistance higher by 2 orders of magnitude) also on the reverse, i.e. the non-implanted side. This is most probably due to the intensive heating of the thin foil during irradiation.

Formation of the conducting carbon cluster network leads also to the decrease of the optical bandgap energy to 2.0 eV (Ne) and 2.75 eV (He) in the case of the largest modification ($\Phi = 5 \times 10^{15}$ cm^{-2}). The average sizes of carbon clusters are also estimated — the number of C atoms in a cluster is found to rise with Φ. It was also found that the sample conductance increases with Φ in the whole considered frequency range (up to 2 MHz) and the $G-f$ curves for $\Phi < 10^{15}$ cm^{-2} follow the Jonscher power law. The dielectric constant of the implanted foils becomes larger with the implantation fluence in the considered f range for all implanted elements, though this effect is the strongest for heavier projectiles like Ar and Ne.

References

[1] Y. Wu, T. Zhang, H. Zhang, X. Zhang, Z. Deng, G. Zhou, *Nucl. Instrum. Methods Phys. Res. B* **169**, 89 (2000).

[2] Y. Wu, T. Zhang, A. Liu, X. Zhang, G. Zhou, *Sci. China E* **46**, 125 (2003).

[3] P. Cottin, R.A. Lessard, E.J. Knystautas, *Nucl. Instrum. Methods Phys. B* **15**, 97 (1999).

[4] E.H. Lee, *Nucl. Instrum. Methods Phys. Res. B* **151**, 29 (1999).

[5] M.F. del Grosso, V.C. Chappa, G. Garcia Bermudez, E. Forlerer, M. Behar, *Surf. Coat. Technol.* **202**, 4227 (2008).

[6] M. Guenther, G. Gerlach, G. Suchaneck, K. Sahre, K.J. Eichhorn, B. Wolf, A. Deineka, L. Jastrabik, *Surf. Coat. Technol.* **158–159**, 108 (2002).

[7] G.R. Rao, K. Monar, E.H. Lee, J.R. Treglio, *Surf. Coat. Technol.* **64**, 69 (1994).

[8] A. Valenza, A.M. Visco, L. Torrisi, N. Campo, *Polymer* **45**, 1707 (2004).

[9] A. Turos, J. Jagielski, A. Piątkowska, D. Bieliński, L. Ślusarski, N.K. Madi, *Vacuum* **70**, 201 (2003).

[10] V. Resta, L. Calcagnile, G. Quarta, L. Maruccio, A. Cola, I. Farella, G. Giancane, L. Valli, *Nucl. Instrum. Methods Phys. Res. B* **312**, 42 (2013).

[11] R. Nathawat, Y.K. Vijay, P. Kumar, P. Kulriya, V. Ganesan, V. Sathe, *Adv. Polym. Technol.* **27**, 143 (2008).

[12] W. Hong, H.J. Woo, H.W. Choi, Y.S. Kim, G. Kim, *Appl. Surf. Sci.* **169-170**, 428 (2001).

[13] S. Arif, M.S. Rafique, F. Saleemi, R. Sagheer, F. Naab, O. Toader, A. Mahmood, R. Rashid, M. Mahmood, *Nucl. Instrum. Methods Phys. Res. B* **358**, 236 (2015).

[14] C. Alvarez, I. Sics, A. Nogales, Z. Dencheva, S.S. Funari, T.A. Ezquerra, *Polymer* **45**, 3953 (2004).

[15] *Handbook of Thermoplastic Polyesters*, Ed. S. Fakirov, Wiley-VCH, Weinheim 2002.

[16] M. Mallick, T. Patel, R.C. Behera, S.N. Sarangi, S.N. Sahu, R.K. Choudhry, *Nucl. Instrum. Methods Phys. Res. B* **248**, 305 (2006).

[17] M. Djebara, J.P. Stoquert, M. Abdesselam, D. Muller, A.C. Chami, *Nucl. Instrum. Methods Phys. Res. B* **274**, 70 (2012).

[18] P.K. Goyal, V. Kumar, R. Gupta, S. Mahendia, A.S. Kumar, *Adv. Appl. Sci. Res.* **2**, 77 (2011).

[19] Y. Sun, C. Li, Z. Zhiyong, W. Liu, S. Yang, *Nucl. Instrum. Methods Phys. Res. B* **135**, 517 (1998).

[20] R. Kumar, M. Goyal, A. Sharma, S. Aggarwal, A. Sharma, D. Kanjilal, *AIP Conf. Proc.* **1661**, 110010 (2015).

[21] M. Chawla, R. Rubi, R. Kumar, A. Sharma, S. Aggarwal, P. Kumar, D. Kanjilal, *Adv. Mater. Res.* **665**, 221 (2013).

[22] A. Tóth, M. Veres, K. Kereszturi, M. Mohai, I. Bertóti, J. Szépvölgyi, *Appl. Surf. Sci.* **257**, 10815 (2011).

[23] Y. Wu, T. Zhang, Y. Zhang, H. Zhang, H. Zhang, G. Zhou, *Sci. China E* **44**, 493 (2001).

[24] P. Malinsky, A. Mackova, V. Hnatowicz, R.I. Khaibullin, V.F. Valeev, P. Slepicka, V. Svorcik, M. Slouf, V. Perina, *Nucl. Instrum. Methods Phys. Res. B* **272**, 396 (2012).

[25] Y. Wu, T. Zhang, Z. Yi, X. Zhang, H. Zhang, X. Zhang, C. Zhou, in: *Proc. 6th Int. Conf. on Solid-State and Integrated-Circuit Technol.*, Ed. B. Li, G. Ru, X. Qu, P. Yu, H. Iwai, IEEE Press and People's Posts & Telecommunications Publishing House, Beijing, 2001, p. 1464.

[26] V. Kumar, R.G. Sonkawade, S.K. Chakarvarti, P. Singh, A.S. Dhaliwal, *Radiat. Phys. Chem.* **81**, 652 (2012).

[27] M. Drabik, K. Dworecki, R. Tańczyk, S. Wąsik, J. Żuk, *Vacuum* **81**, 1348 (2007).

[28] M. Turek, A. Droździel, K. Pyszniak, S. Prucnal, *Nucl. Instrum. Methods Phys. Res. B* **269**, 700 (2011).

[29] M. Turek, A. Drozdziel, K. Pyszniak, S. Prucnal, J. Zuk, *Przeglad Elektrotechniczny* **86**, 193 (2010) (in Polish).

[30] J.F. Ziegler, M.D. Ziegler, J.P. Biersack, *Nucl. Instrum. Methods Phys. Res. B* **268**, 1818 (2010).

[31] K. Kotra-Konicka, J. Kalbarczyk, J.M. Gac, *Chemical and Process Engineering* **37**, 331 (2016).

[32] Th. Lippert, F. Zimmermann, A. Wokaun, *Appl. Spectrosc.* **47**, 1931 (1993).

[33] S. Gupta, D. Choudhary, A. Sarma, *J. Polym. Sci. Part B Polym. Phys.* **38**, 1589 (2000).

[34] A. Mackova, P. Malinsky, R. Miksova, V. Hnatowicz, R.I. Khaibullin, P. Slepicka, V. Svorcik, *Nucl. Instrum. Methods Phys. Res. B* **331**, 176 (2014).

[35] A.K. Jonscher, *Nature* **267**, 673 (1977).

[36] K. Pradhan, R.N.P. Choudhary, B.K. Samantaray, *Int. J. Electrochem. Sci.* **3**, 597 (2008).

[37] K. Prabha, H.S. Jayanna, *Open J. Polym. Chem.* **5**, 47 (2015).